Journal of Colloid and Interface Science 514 (2018) 59–69

Contents lists available at ScienceDirect

Journal of Colloid and Interface Science

journal homepage: www.elsevier.com/locate/jcis

Regular Article

Synthesis and application of bismuth ferrite nanosheets supported functionalized carbon nanofiber for enhanced electrochemical detection of toxic organic compound in water samples

Sukanya Ramaraj [a], Sakthivel Mani [a], Shen-Ming Chen [a,*], Thangavelu Kokulnathan [a], Bih-Show Lou [b,c,*], M. Ajmal Ali [d], A.A. Hatamleh [d], Fahad M.A. Al-Hemaid [d]

[a] Electroanalysis and Bioelectrochemistry Lab, Department of Chemical Engineering and Biotechnology, National Taipei University of Technology, Taipei 10608, Taiwan, ROC
[b] Chemistry Division, Center for General Education, Chang Gung University, Taoyuan 333, Taiwan, ROC
[c] Department of Nuclear Medicine and Molecular Imaging Center, Chang Gung Memorial Hospital, Taoyuan 333, Taiwan, ROC
[d] Department of Botany and Microbiology, College of Science, King Saud University, Riyadh 11451, Saudi Arabia

GRAPHICAL ABSTRACT

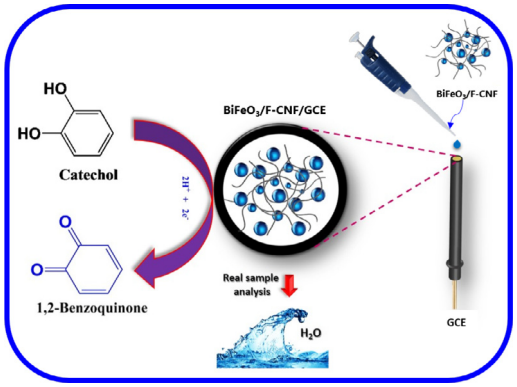

ARTICLE INFO

Article history:
Received 13 September 2017
Revised 2 December 2017
Accepted 5 December 2017
Available online 6 December 2017

Keywords:
Multiferroic material
Bismuth ferrite
Carbon nanofiber
Catechol
Electrochemical sensor
Biosensor

ABSTRACT

Recently, the multiferroic material has fabulous attention in numerous applications owing to its excellent electronic conductivity, unique mechanical property, and higher electrocatalytic activity, etc. In this paper, we reported that the synthesis of bismuth ferrite ($BiFeO_3$) nanosheets integrated functionalized carbon nanofiber ($BiFeO_3$ NS/F-CNF) nanocomposite using a simple hydrothermal technique. Herein, the structural changes and crystalline property of prepared $BiFeO_3$ NS/F-CNF nanocomposite were characterized using Scanning electron microscopy (SEM), Transmission electron microscopy (TEM), X-ray diffraction (XRD), Fourier transform infrared spectroscopy (FT-IR), Raman spectroscopy and X-ray photoelectron spectroscopy (XPS). From this detailed structural evolution, the formation of nanosheets like $BiFeO_3$ and its nanocomposite with F-CNF were scrutinized and reported. Furthermore, the as-prepared $BiFeO_3$ NS/F-CNF nanocomposite modified glassy carbon electrode (GCE) was applied for electrochemical detection of catechol (CC). As expected, $BiFeO_3$ NS/F-CNF/GCE shows excellent electrocatalytic activity as well as 3.44 (F-CNF/GCE) and 7.92 ($BiFeO_3$ NS/GCE) fold higher electrochemical redox response for CC sensing. Moreover, the proposed sensor displays a wide linear range from 0.003 to 78.02

* Corresponding authors at: Chemistry Division, Center for General Education, Chang Gung University, Taoyuan 333, Taiwan, ROC (B.S. Lou).
E-mail addresses: smchen78@ms15.hinet.net (S.-M. Chen), blou@mail.cgu.edu.tw (B.-S. Lou).

https://doi.org/10.1016/j.jcis.2017.12.016

μM with a very low detection limit of 0.0015 μM. In addition, we have validated the real-time application of our developed CC sensor in different water samples.

1. Introduction

Recently, Perovskite structured ferrite has been emerged as an attractive material in different applications such as solar cell, supercapacitor, battery, sensor, fuel cell, hydrogen evolution reaction (HER), and photocatalyst [1–6] because of their enhanced photocatalytic activity, high electrical conductivity, excellent specific capacitance, good chemical stability and non-toxicity. For more than two decades, many perovskite structured ferrites such as $BiFeO_3$, $LaFeO_3$, $PrFeO_3$, $EuFeO_3$, and $GdFeO_3$ have been successfully prepared and applied for aforementioned applications. Among the different perovskite structured materials, $BiFeO_3$ is one of the exclusive multiferroic material due to their possible coupling with a magnetic moment, large polarization, more stability and excellent electrocatalytic property [7–10]. It exhibits combined properties of both ferromagnetism and ferroelectricity with a band gap of around 2.31 eV. Moreover, the diverse structure of $BiFeO_3$ including nanoparticle [11], nanofiber [12], nanoflake [13], nanoflower and nanorod [14,15] have been prepared by using various techniques such as hydrothermal technique, sol-gel method, spray pyrolysis, microwave assisted technique and electrospinning. In these all techniques, hydrothermal synthesis is a promising method to prepare highly crystalline and uniform sized $BiFeO_3$ particles with defined morphology [16]. Moreover, $BiFeO_3$ is used in potential applications such as photocatalyst [17], memory storage [18], gas sensor [19], spintronic devices [20], optic filter [21], energy storage [22] and solar cell [23] due to its remarkable low charge transfer resistance, high specific capacitance, high photocatalytic activity, long cycle stability, considerable electrical conductivity and chemical stability.

Recently, Sarkar et al. reported three dimensional $BiFeO_3$ anchored with TiO_2 for electrochemical energy storage and solar energy conversion with resultant high specific capacitance and excellent photoconversion efficiency [24]. Mushtaqsobhan et al. synthesized $BiFeO_3$ nanofiber for O_2 sensing [25]. The structural studies of $BiFeO_3$ and its application in energy storage and solar energy conversion are well documented but the electrochemical sensor application of $BiFeO_3$ for biomolecules is still demanding. Hence, we attempted to the synthesis of nanosheets like structured $BiFeO_3$ and its application in the electrochemical sensor. In addition, the combination of $BiFeO_3$ with carbon nanomaterials could believe as a possible way to improve its electrocatalytic behavior.

For more than two decades, the carbon materials including graphite, graphene or reduced graphene oxide, mesoporous carbon, carbon nanotube (CNT), fullerene (C60), carbon nanofiber have been widely used as an effective supportive material because of their high surface area, excellent electrical conductivity, exclusive electrocatalytic property and more stability [26–28]. In recent times, CNF has much attention in numerous applications due to its high strength, low density, high metallic conductivity and a larger surface to volume ratio than CNT [29,30]. Moreover, the CNF has cylindrical nanostructure with staking arrangement of graphene sheets and more edge plane defects on its outer wall, which offers effective electron transfer of electroactive molecules [31]. Hence, it is used as an effective electrode material in numerous applications including battery [32], supercapacitor [33] fuel cell [34] and solar cell [35], etc. [36]. However, the insolubility of pristine CNF in water is considering as a major problem for electrode preparation in all aforementioned applications. Recently, the functionalization of CNF is a well-known phenomenon to improve its solubility and also remove the catalytic impurities for enhancing the electrochemical properties by the generation of more anchoring sites and surface reactive groups (carboxylic acid, hydroxyl, and carbonyl groups) on the open end and side walls of CNF. Therefore, the functionalized CNF is a promising carbon material to fabricate the electrode with enhanced electrochemical properties for aforementioned applications.

In this work, we demonstrated the hydrothermal synthesis of $BiFeO_3$ NS/F-CNF nanocomposite and its application towards catechol sensing. In general, the two-dimensional nanostructured materials are so favorable for the electrochemical sensor due to its high electrocatalytic activity and the availability of large surface area [37]. Thus, the two-dimensional nanosheets structure of $BiFeO_3$ and more active sites of F-CNF are available for the preparation of an efficient electrode for electrochemical sensor. As expected, the prepared nanocomposite exhibits better electrochemical response with resultant high sensitivity and selectivity towards the sensing of catechol.

Catechol (CC) is an ortho isomer of benzenediols and classified as a type of phenolic compounds with a molecular formula of $C_6H_4(OH)_2$. This colorless organic compound occurs naturally in fruits and vegetables such as banana, avocado, apple, potatoes, and onion [38]. On other hands, the larger amount of CC (20,000 tons/year) is produced industrially due to its wide applications in pharmaceutical, cosmetics and agriculture, etc. [39]. Moreover, the CC is used as an antioxidant in chemical, photographic, rubber, oil, and dye industries. During the industrial production, the large amount CC was released into the environment. It causes some side effects to human beings such as eye and skin burn, liver injury, paroxysm, and irregular blood pressure [40]. And also, CC was found as an unsafe additive in cosmetics because the continuous exposure of CC on the skin causes the eczematous dermatitis disease [41]. Even the low concentration of catechol induces the DNA damage and affect the human blood cell by changing the function of erythrocytes [42]. Noticeably, the oxidizing agents (enzymes in plants, animals, and bacteria ex: catechol oxidase) oxidized the CC into benzoquinone and form the stable complex with heavy metals, which are the main reason for the toxicity of CC. For example, the DNA strand breakage causes due to the redox reaction between Cu (II) and CC [43]. Hence, the US Environmental Protection Agency (EPA) classified the catechol as a toxic pollutant [44]. For more than two decades, a variety of analytical techniques have been followed to detect the catechol such as High-performance liquid chromatography [45], flow injection [46], spectrophotometric [47], fluorescence [48] and electrochemical technique [49,50]. Among the all, electrochemical technique is a fast, simple, low cost, good sensitivity, and higher selectivity, easy to electrode fabrication and less time-consuming process to determine the target analyte even at a very low concentration in contaminated water/soil/environment [51,52]. As related to the electrochemical techniques, the other techniques have some drawbacks such as high cost, very complex to sample preparation, and time-consuming methods. For the aforementioned reason, the electrochemical technique is considered as a promising method to sense catechol.

2. Experimental section

2.1. Materials and reagents

Bismuth nitrate $Bi(NO_3)_3{\cdot}5H_2O$, carbon nanofiber (CNF, D × L = 100 nm × 20–200 μM, average pore volume = 0.075 cm^3/g), ferric nitrate $Fe(NO_3)_3{\cdot}9H_2O$, citric acid, sodium hydroxide (NaOH), nitric acid (HNO_3), ethanol and all other chemicals were purchased from Sigma Aldrich. The supporting electrolyte 0.05 M phosphate buffer solution (PBS) (pH 7) electrolyte solution was prepared by mixing of 0.05 M Na_2HPO_4 and NaH_2PO_4 and the pH of the electrolytes solution was adjusted by $NaOH/H_2SO_4$. All chemicals reagents were of analytical grade and were used without further purification.

2.2. Hydrothermal synthesis of $BiFeO_3$ NS/F-CNF nanocomposite

The nano-sheet structured $BiFeO_3$ NS/F-CNF nanocomposite was prepared by following stepwise synthesis process. In the first step, the functionalization of CNF was carried out by following acid treatment to enrich its electrical conductivity and solubility by introducing the oxygen functional groups. In the typical experiment, 1 g of CNF was added to the 40 mL of HNO_3/H_2SO_4 (1:3) acid mixture at 50 °C for 8 h with continuous magnetic stirring. Then, the resultant CNF solution was centrifuged and washed with the obvious amount of DD water until the pH value attains around 7. Finally, the resultant product was dried in vacuum oven for overnight [69,70].

In the second step, $BiFeO_3$ NS was prepared by using hydrothermal synthesis method. In this process, 0.2 M of $Bi(NO_3)_3{\cdot}5H_2O$, 0.2 M of $Fe(NO_3)_3{\cdot}9H_2O$, F-CNF (1 mg/1 mL) were prepared in 50 mL of DD water and kept in magnetic stirring for 15 min. Afterwards, 2 mL of 2 M of HNO_3 and 0.2 M of citric acid in 5 mL of DD water were prepared and added to the above mixture. The obtained black solution was transferred into stainless steel Teflon lined autoclave and kept in 200 °C for 6 h. After the temperature treatment, the autoclave was allowed to cool at room temperature. The final product was gathered using a centrifuge allowed for many time washing with ultra-pure water and absolute ethanol, final product was dried in vacuum oven at 70 °C. The $BiFeO_3$ NS was also prepared by following the same above procedure without F-CNF for electrochemical comparison studies.

2.3. Characterization

Scanning electron microscopy (SEM) was performed using Hitachi S-3000H electron microscope. TEM (JEOL 2100F) was used to investigate the morphology and nanostructure of nano-sheet $BiFeO_3$/F-CNF. XRD characterization was carried out using XPERT-3 diffract meter with Cu Kα radiation (K = 1.54 Å). Fourier transform infrared spectroscopy (FTIR) measurement was recorded using JASCO FT/IR-6600. Raman spectroscopy was a recorded using WITech CRM200 confocal microscopy Raman system with a 488 NM laser. The chemical state of Bi, Fe, and O was recorded using X-ray Photoelectron Spectroscopy (XPS, Thermo scientific multi lab 2000). Electrochemical impedance spectroscopy (EIS) was performed using IM6ex ZAHNER impedance measurement unit. The cyclic voltammetry (CV) and differential pulse voltammetry (DPV) studies were performed using CHI750A electrochemical analyzer. The conventional three-electrode system was utilized in these all electrochemical studies. The glassy carbon electrode (GCE) was used as a working electrode, a saturated Ag/AgCl electrode as a reference electrode and a platinum wire as the auxiliary electrode. All the electrochemical measurements were carried out at room temperature.

2.4. Fabrication of $BiFeO_3$ NS/F-CNF modified GCE

The $BiFeO_3$ NS/F-CNF dispersion was prepared by dispersing of 1 mg $BiFeO_3$ NS/F-CNF in 1 mL ethanol and sonicated for 15 min. Subsequently, as prepared 6 μL of $BiFeO_3$ NS/F-CNF suspension was drop cast on GCE surface and dried in the oven at 45 °C. After that, the dried GCE was gently washed with DD water to remove the loosely bounded molecules on the GCE surface. Finally, the obtained $BiFeO_3$ NS/F-CNF modified GCE was used for further electrochemical studies.

3. Result and discussion

3.1. Characterization of $BiFeO_3$ NS/F-CNF nanocomposite

The morphological studies were recorded for as prepared $BiFeO_3$ NS/F-CNF nanocomposite using SEM and TEM analysis. Fig. 1(A) displays the clear SEM image of two-dimensional nanosheets like a structure of $BiFeO_3$ formed in following hydrothermal synthesis. In general, two-dimensional nanomaterials exhibit high electrocatalytic activity, which is so favorable for an efficient electrochemical sensing of phenolic compounds.

Fig. 1(B) shows the fiber-like structure of carboxylic acid functionalized CNF. In acid treatment, the length of the CNF was shortening with least side wall damages, which facilitate high-level solubility of CNF in water [53]. To enrich the electrochemical activity of $BiFeO_3$ NS, which was hydrothermally integrated with F-CNF.

The formation of this new type of nano-composite was strongly confirmed by observing Fig. 1(C) and (D). It clearly shows that the $BiFeO_3$ nanosheets were fully surrounded by F-CNF. To provide the strong evidence for nanosheets formation of $BiFeO_3$ and its nanocomposite, TEM analysis also was recorded. Fig. 2(A) and (B) shows the different magnified TEM images of transparent $BiFeO_3$ nanosheets. Thus, the average diameter of the nanosheets was founded as 416.75 nm as shown in Fig. 2(B) (inset). Furthermore, Fig. 2(C) and (D) shows the different magnified TEM images of F-CNF. It clearly displays that the surface of F-CNF with stacking arrangement of graphene sheets. The open end of F-CNF was formed in acid treatment, which enhances its solubility. In addition, the average diameter of the F-CNF also measured to be 90.54 nm (Fig. S1). Fig. 2(E) and (F) shows the TEM images of $BiFeO_3$ NS/F-CNF nanocomposite. The result evidently confirms the effective integration of $BiFeO_3$ NS and F-CNF.

The crystalline phase of $BiFeO_3$ nanosheets and $BiFeO_3$ NS/F-CNF nanocomposite was confirmed by XRD analysis. The several major diffraction peaks were observed at 24°, 32°, 36.6°, 40.9°, 46.7°, 49.7°, 54.2°, 55.1° and 58.6° with corresponding lattice planes such as (0 1 2), (1 0 4), (1 1 0), (0 0 6), (2 0 2), (0 2 4), (1 1 6), (1 2 2), (0 1 8) and (2 2 4) as shown in Fig. 3. The XRD pattern confirmed the rhombohedra perovskite structure of $BiFeO_3$ nanosheets with *R*3*c* space group. The obtained XRD pattern of $BiFeO_3$ NS is strongly assigned to the standard data (JCPDS NO: 20-0169) [24]. Moreover, the sharp diffraction peaks are indicating the high crystalline purity of $BiFeO_3$ nanosheets. Fig. 3 (inset) shows the clear XRD pattern of F-CNF with major diffraction peak at $2\theta = 25°$ and 43.6° for corresponding lattice plane (0 0 2) and (1 1 0) respectively. The successful formation of the nanocomposite was confirmed by observing the diffraction peaks of both $BiFeO_3$ nanosheets and F-CNF in XRD pattern of nanocomposite. There are no other peaks were observed related to bismuth oxide, which confirms that the prepared $BiFeO_3$ NS is pure.

FT-IR spectroscopy is known as a promising technique to understand the formation of nanocomposite with respect to the resultant vibrational and stretching band for corresponding functional groups. The FT-IR spectrum of $BiFeO_3$ nanosheets, CNF and $BiFeO_3$

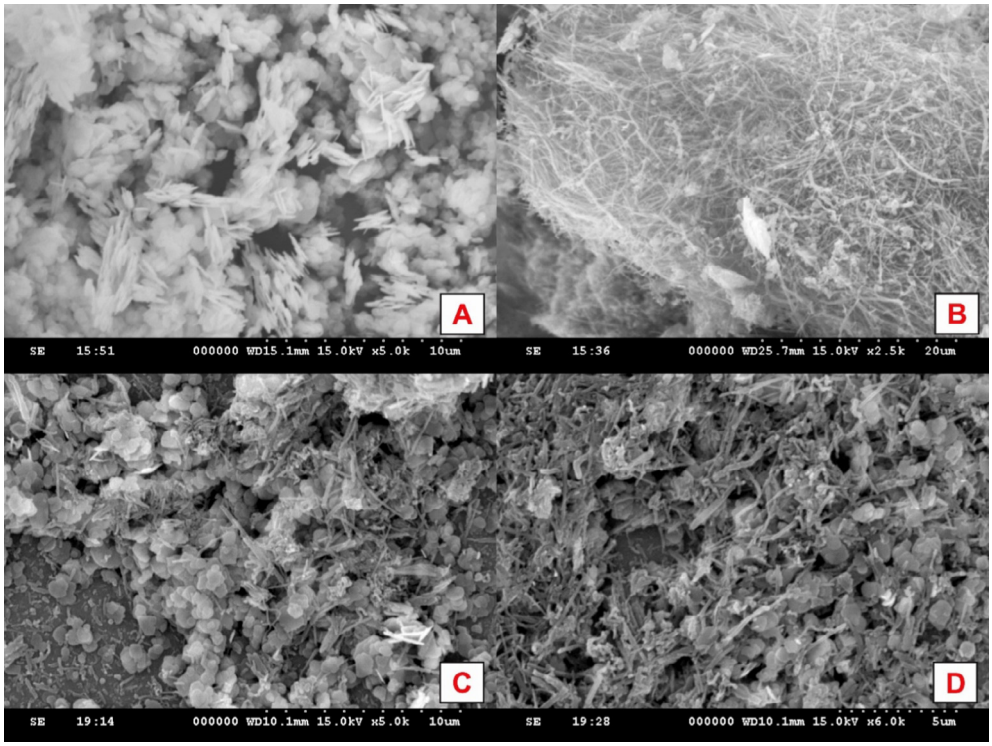

Fig. 1. SEM images of (A) $BiFeO_3$ NS, (B) F-CNF and (C, D) $BiFeO_3$ NS/F-CNF.

NS/F-CNF nanocomposite are shown in Fig. 4. The FT-IR spectra of $BiFeO_3$ nanosheets with a broadband at 3411.86 cm^{-1} for asymmetric and symmetric stretching of bond H_2O and OH. The band at 1627 cm^{-1} was observed due to the bending vibration of H_2O. The octahedral FeO_6 groups in the perovskite compounds exhibit the band at 548.38 and 433 cm^{-1} for corresponding Fe—O stretching and O—Fe—O bending vibrations [9]. The FT-IR spectra of F-CNF with the characteristic bands at 1720, 1047 and 1227 cm^{-1} for corresponding oxygen functional groups C═O, C—OH and C—O—C respectively. It implies the successful carboxylic acid functionalization of CNF [56]. The corresponding maximized FT-IR spectrum of F-CNF is shown in Fig. 4 (inset).

For the comparison, Fig. S2 shows the FT-IR spectrum of pristine CNF with weakly observed peaks. Thus, the introduction of oxygen functional groups in acid treatment can effectively enhance the solubility of CNF. Moreover, the formation of $BiFeO_3$ NS/F-CNF nanocomposite due to the presence of corresponding bands of both $BiFeO_3$ and F-CNF in FT-IR pattern of the nanocomposite. The Raman analysis also evidently confirms the functionalization of CNF through the variation in the relative intensity of D band and G band. The Raman spectra of both CNF and F-CNF (Fig. S3) exhibit two well-defined D band and G band at 1368 cm^{-1} and 1617 cm^{-1} respectively. In general, the D band ascribed due to disordered (sp^2 bonded sites) nature of the graphitic structure and G band is due to the C—C stretching in a graphitic material. The Raman spectra of F-CNF shows the increasing intensity of D band due to the formation of defect on the surface of CNF during functionalization process. The intensity ratio of the D band to the G band (I_D/I_G) is often used to estimate the defect concentration in carbon materials. The I_D/I_G ratio of CNF is 0.42 lower than 1.78 of F-CNF are confirming the functionalization process.

The electronic state of the elements in $BiFeO_3$ NS was successfully analyzed using XPS technique and demonstrated in Fig. 5. Herein, Fig. 5A shows the survey spectrum of $BiFeO_3$ NS with major characteristic peaks of Bi, Fe and O elements, where the peak of C is a reference. It strongly confirms the $BiFeO_3$ NS contains Bi, Fe and O element in near-surface range. Fig. 5(B)–(D) shows the high-resolution XPS spectra of Bi 4f, Fe 2p, and O 1s respectively. The XPS spectra of Bi 4f shows the two major peaks at a binding energy of 158.62 and 163.52 eV for corresponding Bi $4f_{7/2}$ and Bi $4f_{5/2}$ states respectively. In addition, the XPS spectra of Fe 2p shows the peak at 711.06 for Fe $2p_{3/2}$ state and the transition peaks on higher energy state at 723.44 are strongly assigned to Fe $2p_{1/2}$ state. The two satellite peaks at 718.62 is strongly indicated the divalent state of Fe in $BiFeO_3$ NS. The XPS spectra of O 1s was classified into three components peak such as OI, OII, and OIII respectively. In general, OI due to the BE of oxygen adsorbed to the transition metal, OII is assigned to low coordinated surface oxygen ions and OIII represent the surface contamination. Thus, XPS analysis confirms that the formation of $BiFeO_3$ NS and the distribution of Bi, Fe, and O with corresponding electronic states, which is good agreement with other previously reported literature [68].

3.2. Electrochemical property of $BiFeO_3$ NS/F-CNF/GCE

Electrochemical impendence spectroscopy (EIS) is a versatile method to characterize the electrical properties of electrode materials and measure interfacial properties between electrode surfaces and electrolyte. Fig. 6 shows the EIS curve of bare GCE, $BiFeO_3$/GCE, F-CNF/GCE and $BiFeO_3$ NS/F-CNF/GCE in 5 mM of $[Fe(CN)6]^{3-/4-}$ containing 0.1 M KCl in the frequency range from 0.1 Hz to 100 kHz at an AC applied a potential of 10 mV. The obtained results are represented in the form of Nyquist plots. The impedance data were fitted to the Randles circuit shown in the inset of Fig. 6, where R_{ct} is charge transfer resistance, R_s is electrolyte resistance, Z_w is Warburg impedance and C_{dl} is double layer capacitance. In the Randles circuit, the Rct and Warburg impedance can be found to be parallel to C_{dl} which results in a semicircle in the Nyquist plots. The diameter of the semicircle is equal to the R_{ct} value which is revealing of the electron transfer kinetics of the redox probe at

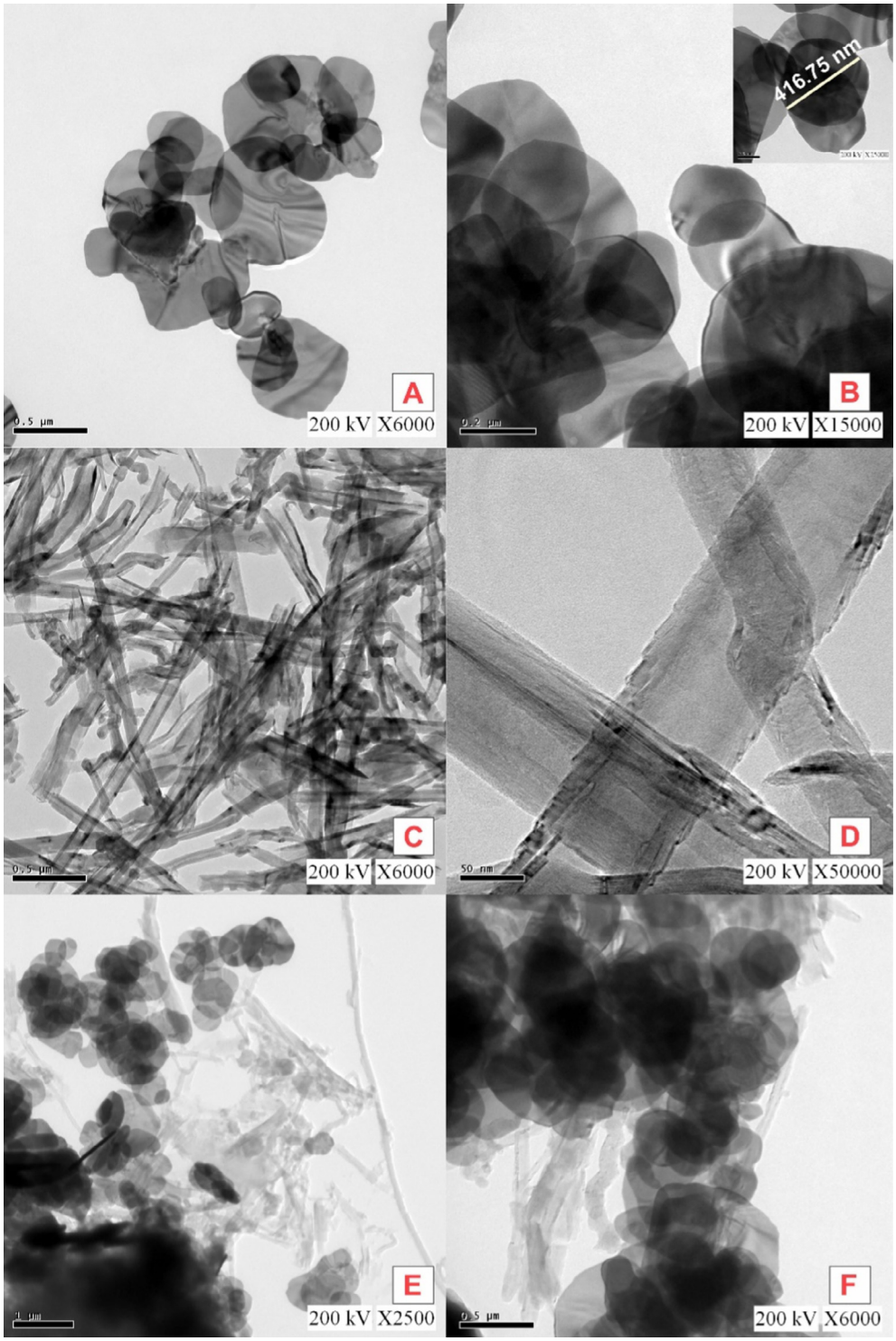

Fig. 2. TEM images of (A, B) $BiFeO_3$ NS (C, D) F-CNF and (E, F) $BiFeO_3$ NS/F-CNF.

the electrode/electrolyte interface. The impedance data of GCE, $BiFeO_3$/GCE, F-CNF/GCE and $BiFeO_3$ NS/F-CNF/GCE show two distinct regions viz. a linear part at low-frequency region and semicircular part at high-frequency region. The semicircle corresponds to the electron transfer process, and its diameter is equivalent to the charge transfer resistance (R_{ct}). The linear part at lower frequencies corresponds to a diffusion-limited process. From the experimental results, the R_{ct} value of GCE, $BiFeO_3$/GCE, F-CNF/GCE and $BiFeO_3$ NS/F-CNF/GCE were calculated about 95 Ω, 107.89 Ω, 2 Ω and 16 Ω, respectively. Thus, the integration of F-CNF effectively enhances the low charge transfer resistance of the reported nanocomposite modified GCE.

In addition, the CV technique also was recorded to calculate the electron transfer kinetics and active surface area of $BiFeO_3$ NS/F-CNF/GCE based on basic electrochemical redox process of $[Fe(CN)_6]^{3-/4-}$. Fig. S4(A) displays the CV profile of bare GCE, $BiFeO_3$/GCE, F-CNF/GCE and $BiFeO_3$ NS/F-CNF/GCE in 5 mM of $[Fe(CN)_6]^{3-/4-}$ contains 0.1 M of KCl at 50 mV s^{-1}. Herein, $BiFeO_3$

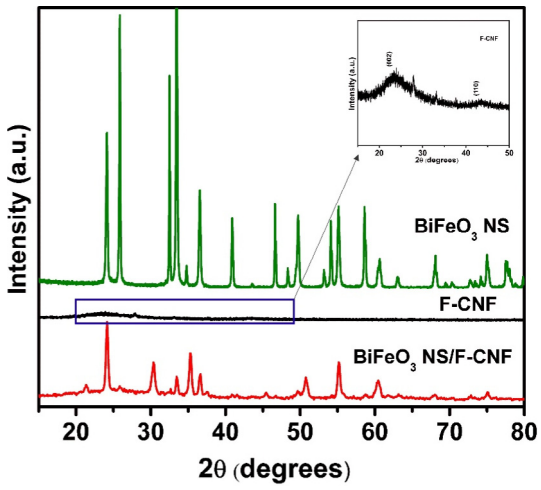

Fig. 3. XRD pattern of $BiFeO_3$ NS, F-CNF and $BiFeO_3$ NS/F-CNF nanocomposite.

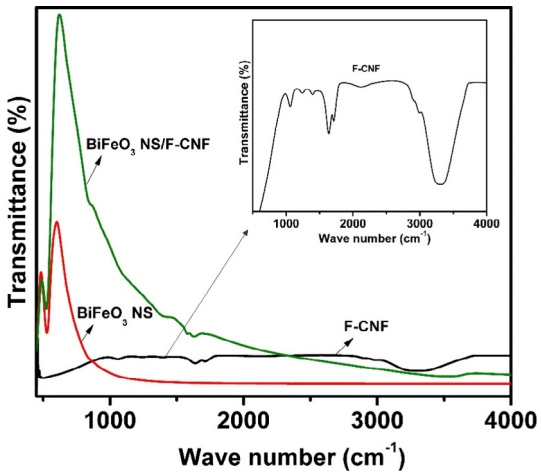

Fig. 4. FTIR spectra of $BiFeO_3$ NS, F-CNF and $BiFeO_3$ NS/F-CNF nanocomposite.

NS/F-CNF/GCE shows the higher reversible redox peak current response with lowest peak potential separation (ΔEp = 0.106 V). As the result of this experiment, the lowest value of ΔEp and higher redox peak current response are indicating that $BiFeO_3$ NS/F-CNF/GCE has faster electron transfer kinetics than that of other modified electrodes. In addition, the active surface area of $BiFeO_3$ NS/F-CNF/GCE was studied in $[Fe(CN)_6]^{3-/4-}$ by varying scan rate from 10 to 100 mV s^{-1} as shown in Fig. S4(B), which clearly shows the increasing redox peak current response by increasing scan rate. The corresponding linear calibration was plotted for the square root of the scan rate vs. redox peak current and shown in Fig. S4(C), It indicates that the overall electrochemical redox process of $[Fe(CN)_6]^{3-/4-}$ is a diffusion controlled process. Finally, the active surface area of the modified electrodes was calculated by using the Randles-Sevick equation:

$$I_p = 2.69 \times 105\ A\ D^{1/2} n^{3/2} \gamma^{1/2} C \quad (1)$$

where I_p is the peak current, D is the diffusion coefficient of ferricyanide solution ($cm^2\ s^{-1}$), n is the number of electron transfer (n = 1), γ is the scan rate (V s^{-1}), and C is the concentration of ferricyanide in bulk solution. By using the Eq. (1), the active surface area was calculated to be 0.033, 0.080, 0.093 and 0.110 cm^2 for bare GCE, $BiFeO_3$/GCE, F-CNF/GCE and $BiFeO_3$ NS/F-CNF/GCE, respectively. Thus, $BiFeO_3$ NS/F-CNF/GCE is found as a suitable electrode material with higher electron transfer kinetics and higher active surface area, which can offer the excellent electrochemical activity towards the electrochemical detection of CC.

3.3. Electrochemical behavior of $BiFeO_3$ NS/F-CNF/GCE nanocomposite towards the detection of CC

The electrochemical behavior of $BiFeO_3$ NS/F-CNF nanocomposite modified GCE was studied and compared with other modified electrodes using CV technique. Fig. 7(A) shows the CV curve of $BiFeO_3$ NS/F-CNF/GCE, $BiFeO_3$/GCE, F-CNF/GCE and bare GCE with the presence of CC (100 μM) in N_2 saturated 0.05 M PBS (pH 7) at a scan rate of 50 mV s^{-1}. The result of this experiment, $BiFeO_3$ NS/F-CNF/GCE exhibits enhanced lower oxidation (E_{pa} = 0.25) and reduction potential (E_{pc} = 0.18) with higher anodic (I_{pa} = 49.73) and cathodic peak current (I_{pc} = 32.6) for sensing of CC, which is 3.44 and 7.92 fold higher redox current response when compared to the other modified electrodes such as F-CNF and $BiFeO_3$ NS modified GCE. The two-dimensional nanostructure of $BiFeO_3$ NS and the presence of more active edge sites of F-CNF can facilitate the electrocatalytic activity for $BiFeO_3$ NS/F-CNF nanocomposite modified GCE. Herein, the electronic structure of Fe ions (coordinately unsaturated d orbitals because of the missing oxygen legends) into consideration, one may expect a high sensitivity in $BiFeO_3$ because the dangling bonds can provide geometrically and electronically favorable sites for molecule chemisorption, which is an important prerequisite for sensing property of $BiFeO_3$ towards the detection of CC [77]. Whereas the CC interacts with F-CNF surface through the hydrogen bonding between their hydroxyl groups and also the π-π interactions between the aromatic moieties [78]. Therefore, the combine sensing properties of $BiFeO_3$ and F-CNF facilitate the excellent electrochemical detection of CC.

We have also examined the electrochemical redox behavior of $BiFeO_3$ NS/F-CNF with presence and absence of CC (100 μM) as shown in Fig. 7(B). In absence of CC, there is no redox response observed at $BiFeO_3$ NS/F-CNF. It reveals that the $BiFeO_3$ NS/F-CNF modified GCE electrode is electrochemically inactive at a particular potential window. On the other hand, the sharp redox response was observed for the presence of CC (100 μM). The result scrutinized that the as reported $BiFeO_3$ NS/F-CNF modified GCE electrode is a suitable active electrode material for sensing of CC. The possible electrochemical redox mechanism is also shown in Scheme 1.

Fig. 7(C) implies the scan rate dependent electrocatalytic behavior of $BiFeO_3$ NS/F-CNF modified GCE in N_2 saturated 0.05 M PBS (pH 7) solution containing CC (100 μM) by varying scan rate from 20 to 200 mV s^{-1}. As expected, the linear increments of redox peak current I_{pa} and I_{pc} were observed for increasing scan rate. Thus, we concluded that the redox peak current of CC is linearly dependent on varying scan rate.

Herein, the linear regression plot was drawn for the scan rate vs. oxidation and reduction peak current of CC with regression equations as I_{pa} (μA) = 0.653 A/mV s^{-1} + 27.061 μA (R^2 = 0.9904) and I_{pc} (μA) = −0.6126 A/mV s^{-1} − 21.04 μA (R^2 = 0.9906) as shown in Fig. 7(D). The results indicate that the electrochemical behavior of CC at $BiFeO_3$ NS/F-CNF modified GCE is a typical surface controlled diffusion process. Fig. 8(A) shows the CV curve of $BiFeO_3$ NS/F-CNF modified GCE for varying the concentration of CC from 0 to 180 μM in N_2 saturated 0.05 M PBS (pH 7) at a scan rate of about 50 mV s^{-1}. The significant electrocatalytic activity of modified $BiFeO_3$ NS/F-CNF modified GCE can understand by observing the linear increment in redox current for the addition of CC.

Moreover, we have studied the influence of the pH of electrolyte towards the electrochemical sensing of CC at $BiFeO_3$ NS/F-CNF modified GCE. Fig. 8(B) shows the CV curve of $BiFeO_3$ NS/F-CNF modified GCE for the addition of CC (100 μM) in N_2 saturated 0.05 M PBS (pH = 3, 5, 7, 9 and 11) at scan rate of 50 mV s^{-1}. From

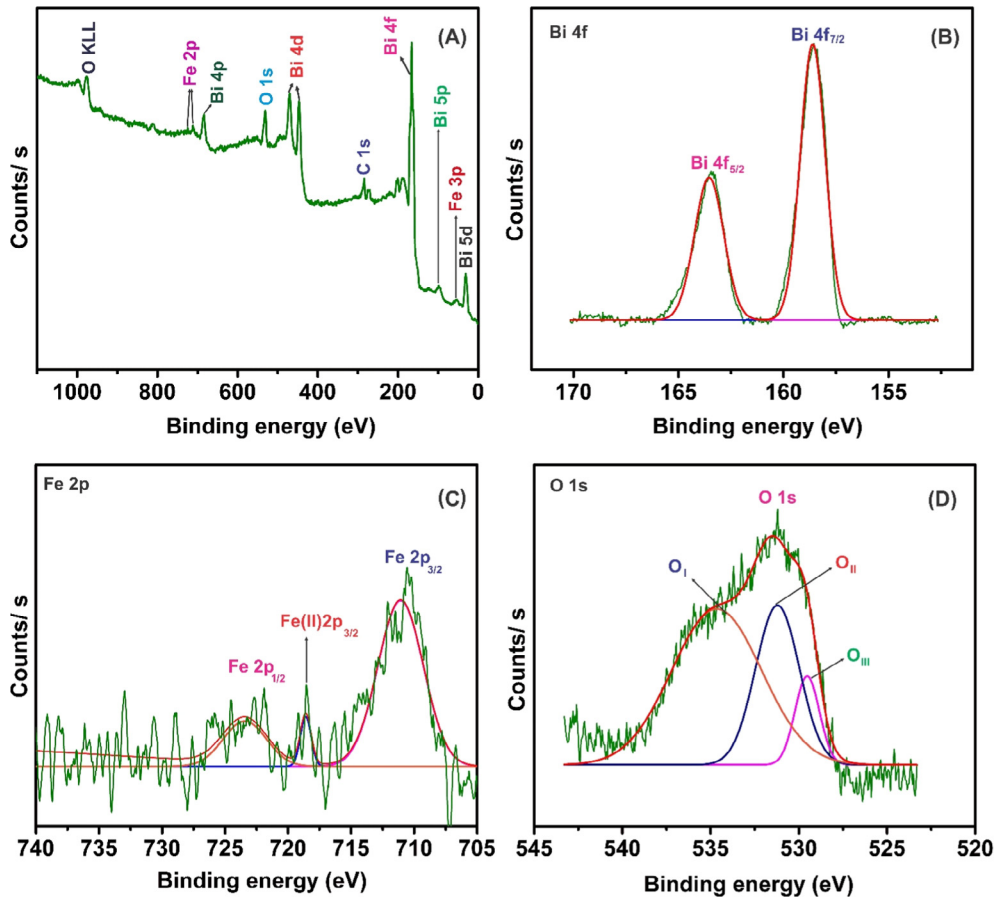

Fig. 5. (A) The full XPS scan and high resolution of $BiFeO_3$ NS, XPS spectra of (B) Bi 4f, (C) Fe 2p and (D) O 1s.

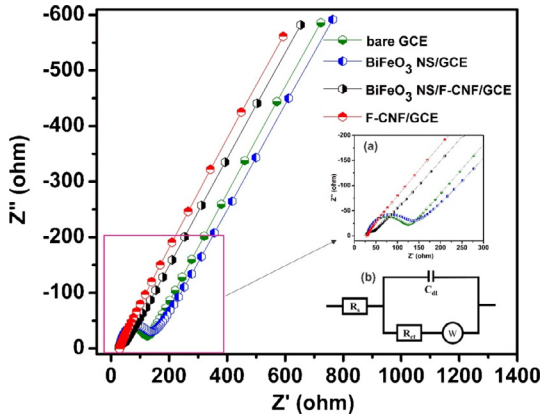

Fig. 6. EIS curve of bare GCE, $BiFeO_3$ NS, F-CNF and $BiFeO_3$/F-CNF in 5 mM of $[Fe(CN)6]^{3-/4-}$ contain 0.1 M of KCl in the frequency range from 0.1 Hz to 100 kHz. Inset: (a) high magnified image of EIS curves. (b) Randles circuit model.

this Fig. 8(B), the anodic and cathodic peak potentials are shifted towards the direction of negative potential upon increasing the pH from 3 to 11. The result indicates that the protons are involved in the oxidation of CC. Moreover, Fig. 8(C) shows the linear regression plot was drawn for pH vs. oxidation potential (E_{pa}) with the calculated slope value of 45.7 mV pH^{-1}, which is relatively close to an anticipated Nernstian value of 59 mV pH^{-1} at 25 °C for an equal number of proton and electron transfer process. In addition, Fig. 8(D) shows regression plot for pH vs. oxidation current (Ipa) of CC. In this plot, the maximum oxidation peak current observed for pH 7 compared to another pH of the solution. Hence, the pH 7 was selected as an optimum pH level of electrolyte solution for electrochemical sensing of CC.

Differential Pulse Voltammetry (DPV) technique was performed to provide the sensitive electrochemical behavior of $BiFeO_3$ NS/F-CNF modified GCE. It is considered as an extensive analytical technique method to determine the primary electrochemical parameters such as the limit of detection (LOD), linear range and sensitivity, which are reveals the relative electrochemical activity of modified electrodes. Hence, DPV technique was employed for the electrode in N_2 saturated 0.05 M PBS (pH 7). Fig. 9 shows the DPV curve with the linear increment of oxidation peak current (I_{pa}) over the addition of CC from 0.003 to 145.91 μM. The linear equation for the calibration plot is I (μA) = 1.6728 + 2.686C (μM) and the R^2 is 0.9943 (Fig. 9(inset)). The sensitivity of the sensor is 15.20 μA μM^{-1} cm^{-2} and was calculated using the slope of the calibration plot/electrochemically active surface area (0.11 cm^2) of the $BiFeO_3$/F-CNF/GCE. Finally, the limit of detection (LOD) of CC at $BiFeO_3$ NS/F-CNF modified GCE was calculated to be 0.0015 μM. Moreover, the analytical parameters such as LOD and linear range of $BiFeO_3$ NS/F-CNF modified GCE towards the sensing of CC were compared with other reported modified electrodes as shown in Table 1. From the comparison table, $BiFeO_3$ NS/F-CNF modified GCE was found with very low LOD, which indicates that the $BiFeO_3$ NS/F-CNF modified GCE is an effective electrode for electrochemical detection of CC.

3.4. Selectivity and stability of proposed sensor

Selectivity and stability are important factors for a unique electrochemical sensor. In order to observe the selectivity of CC at

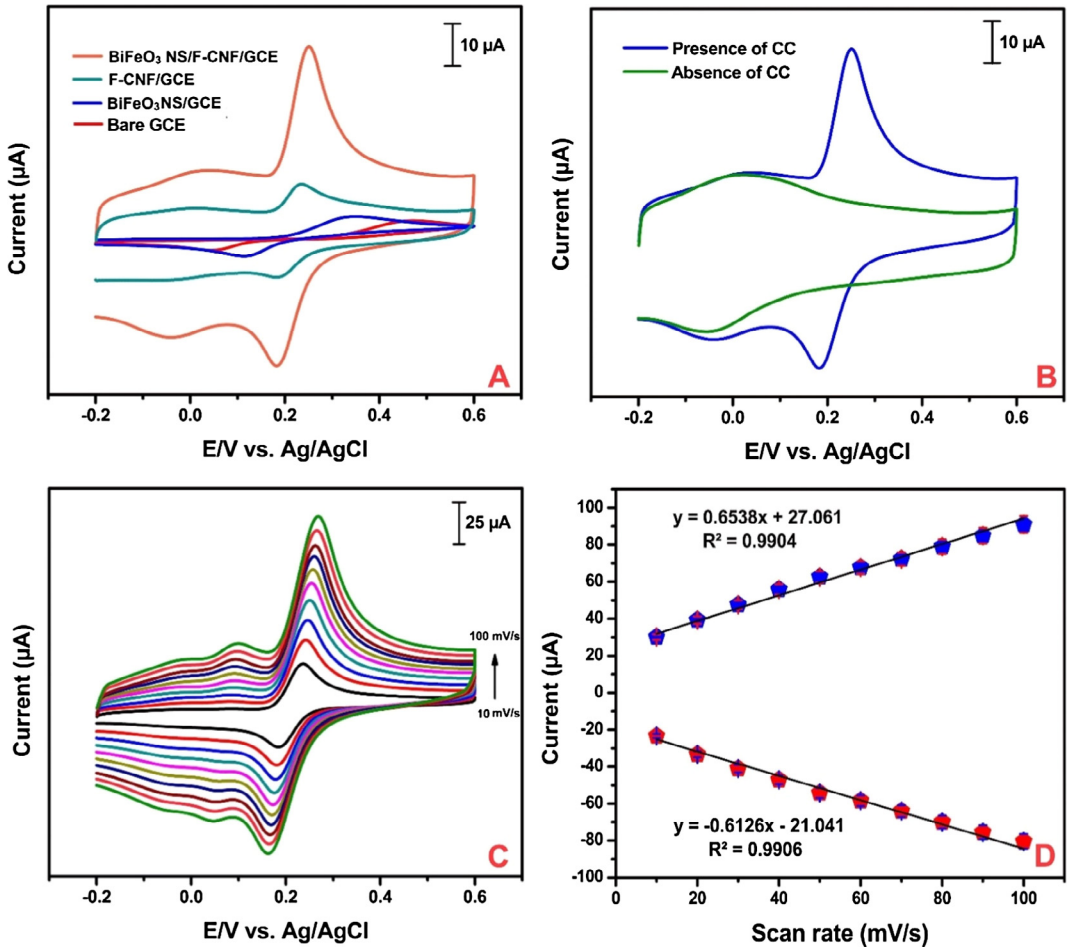

Fig. 7. (A) CV behavior of bare GCE, $BiFeO_3$ NS/GCE, F-CNF/GCE and $BiFeO_3$ NS/F-CNF/GCE in the presence of CC (100 μM) containing N_2 saturated 0.05 M PBS (pH 7) at a scan rate of 50 mV s^{-1}, (B) presence and absence of CC (100 μM) at $BiFeO_3$ NS/F-CNF/GCE in N_2 saturated 0.05 M PBS (pH 7) at scan rate of 50 mV s^{-1}, (C) CV curve of the $BiFeO_3$ NS/F-CNF/GCE in N_2 saturated 0.05 M pH 7.0 containing CC (100 μM) by varying scan rate from 10 to 100 mV s^{-1}, (D) the calibration plot for scan rate vs. oxidation and reduction peak current.

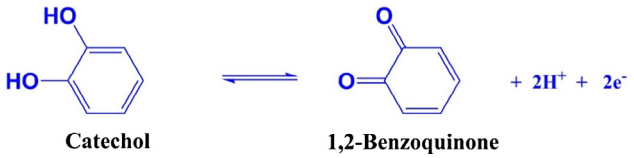

Scheme 1. The electrochemical mechanism of cathecol.

$BiFeO_3$ NS/F-CNF modified GCE, which was tested using DPV technique in N_2 saturated 0.05 M of PBS (pH 7). A typical error analysis was calculated for 10 μM of CC and the addition of other electroactive interferences such as hydroquinone (HQ), resorcinol (RS), 4-aminophenol (4-AP), dopamine (DA), 2-aminophenol (2-AP), 2-chlorophenol (2-CP) and phenol (Ph) as shown in Fig. S5. There is an only negligible percentage of error was observed for addition of interfering compounds. Hence, $BiFeO_3$ NS/F-CNF modified GCE was identified as a sufficient electroactive material for selective sensing of CC. Furthermore, $BiFeO_3$ NS/F-CNF composite modified GCE electrode was exposed to stability test in N_2 saturated 0.05 M PBS (pH 7) containing 100 μM of CC at a scan rate of 50 mV s^{-1} for 100 consecutive cycles as shown in Fig. S6(A). The reported $BiFeO_3$ NS/F-CNF composite modified GCE exhibits 87.5% of its initial oxidation current at 100th cycle which indicates the unique stability of $BiFeO_3$ NS/F-CNF composite modified GCE towards the electrochemical sensing of CC.

3.5. Reproducibility, repeatability and storage stability of proposed sensor

To investigate the reproducibility of as reported sensor, five individual $BiFeO_3$ NS/F-CNF composite modified GCE electrodes were prepared and subjected to individual CV measurement with the presence of CC (100 μM). In result, the unique reproducibility of the reported sensor was found by recording the RSD value about 2.78% and the corresponding bar diagram is shown in Fig. S6(B). Moreover, repeatability of the sensor was analyzed for single $BiFeO_3$ NS/F-CNF composite modified GCE by performing ten successive measurements using CV in N_2 saturated 0.05 M PBS (pH 7) containing CC (100 μM) at a scan rate of 50 mV/s. As a result, the RSD examined to be 2.5%, which illustrate the better repeatability of $BiFeO_3$ NS/F-CNF composite modified GCE towards CC sensing. The corresponding bar diagram is shown in Fig. S6(C). Storage stability also recorded for the reported sensor, which was stored in N_2 saturated 0.05 M PBS (pH 7) for 15 days. The continuous measurement was carried out and monitored the variation in oxidation current of CC for the three-day interval. The reported sensor exhibits its 85.6% of initial oxidation current after 15 days storage which indicates the appreciable storage stability of the $BiFeO_3$ NS/F-CNF composite modified GCE. The corresponding bar diagram is shown in Fig. S6(D).

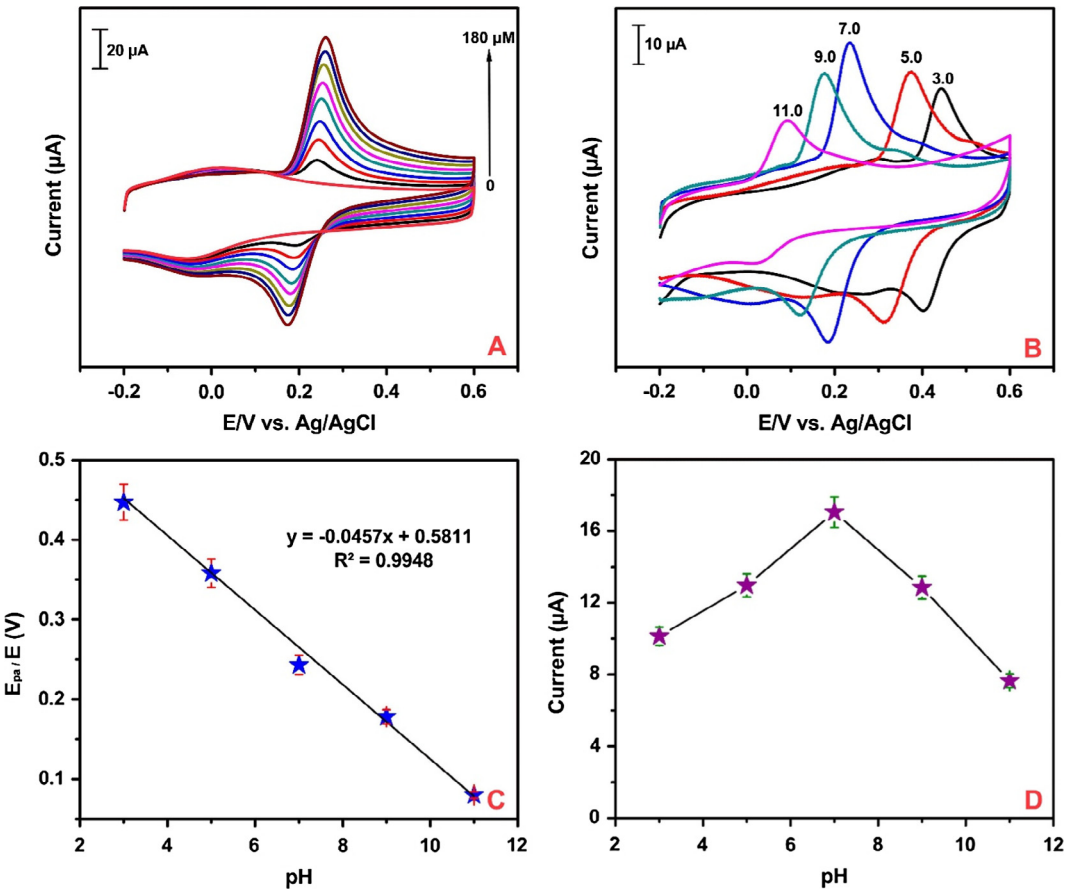

Fig. 8. (A) CV curve of $BiFeO_3$ NS/F-CNF/GCE by varying the concentration of CC (0–180 μM) in N_2 saturated 0.05 M PBS (pH 7) at scan rate of 50 mV s^{-1}, (B) The effect of pH (3–11) of the electrolyte solution at $BiFeO_3$/F-CNF/GCE with presence of CC (100 μM). (C) The corresponding calibration pH vs. plots of oxidation peak potential and (D) pH vs. oxidation peak currents.

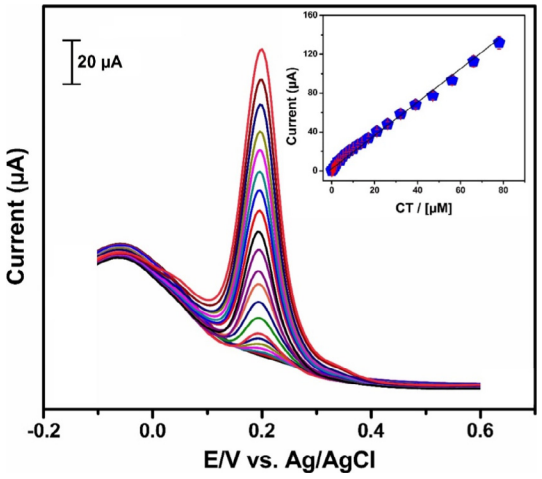

Fig. 9. DPV response of $BiFeO_3$ NS/F-CNF/GCE in N_2 saturated 0.05 M PBS (pH 7) with successive addition of various CC ranging from 0.003 to 145.91 μM. Inset: the corresponding liner regression plot for concentration vs. anodic current.

Table 1
Comparison of different modified electrode for electrochemical sensing of CC.

Electrode	Linear range (μM)	LOD (μM)	Reference
GO@PDA-AuNPs	0.3–67.55	0.015	[54]
Cu-PPy	0.05–1000.0	0.010	[55]
$Au/Ni(OH)_2$/rGO	0.4–33.8	0.13	[56]
Au-G/GCE	1.0–100.0	0.15	[57]
3-APBA-PTCA-CNTs	0.5–30.0	0.1	[58]
ZnS/NiS@ZnS/L-C/AuNPs	0.5–400.0	0.071	[59]
GR–TiO_2	0.5–100.0	0.087	[60]
NCNT@CNF	0.08–350.0	0.02	[61]
GO-M-MnO_2	0.03–1.0	10.0	[62]
Fc/APTMS/GO	3.0–112.0	1.1	[63]
CNF-Bi	3.0–20.0	0.2	[64]
CNCS-RGO	1.0–400.0	0.4	[65]
GNPs/CNF/Au	5.0–350.0	0.36	[66]
$CePO_4$	0.20–40.0	0.10	[67]
MWCNT-NF-PMG	0.03–1.19	5.8	[71]
PM-AuNPs	0.5–175.5	0.011	[72]
GO@PDA-AuNPs	0.3–67.55	0.015	[73]
AC	0.005–0.1	0.002	[74]
GR/CNF/SPCE	0.2–209.7	0.085	[75]
GO/PM	0.03–138	0.008	[76]
$BiFeO_3$/F-CNF	0.003–78.02	0.0015	This work

3.6. Real time application

The practical applicability of $BiFeO_3$ NS/F-CNF modified GCE was also analyzed using DPV techniques. For this experiment, tap and river water were collected and used as the real samples without any pretreatment. Each sample were tested for five times (n = 5). Further, the experiment was performed by adding tap and river water without containing CC in N_2 saturated 0.05 M PBS (pH 7). There is no obvious response was recorded. Afterwards, the known concentrations of CC were spiked into the water samples then directly used for real sample analysis. Here, the standard addition method was followed to measure the recoveries. In result of this experiment, the CC spiked real samples were effectively estimated

Table 2
Determination of CC in different water sample using $BiFeO_3$ NS/F-CNF modified GCE (n = 5).

Sample	Added (μM)	Found (μM)	Recovery (%)	RSD (%)
Tap water	2	1.96	98	4.86
	4	4.02	100.5	3.45
	6	5.85	97.5	3.66
River water	2	2.06	103	2.48
	4	4.2	105	3.62
	6	5.91	98.5	1.25

by $BiFeO_3$ NS/F-CNF modified GCE. The obtained recovery values are ranging from 97.5 to 105% and presented in Table 2. The appreciable result implies that the reported $BiFeO_3$ NS/F-CNF modified GCE is a promising electrode material for electrochemical sensing of CC was proved in real sample analysis.

4. Conclusion

In conclusion, we have prepared $BiFeO_3$ NS/F-CNF nanocomposite using a hydrothermal method and used as an electrode material for electrochemical sensing of CC. numerous techniques such as SEM, TEM, XRD, FTIR, and EIS were performed to characterize the surface morphology, crystallinity and other physio-electrochemical properties of $BiFeO_3$ NS/F-CNF nanocomposite. Moreover, CV and DPV techniques were used to analyze the electrocatalytic activity of $BiFeO_3$ NS/F-CNF nanocomposite modified GCE towards the sensing of CC. In result, the reported sensor exhibits the selective determination of CC with the ultra-low detection limit of CC than previously reported works. The substantial practical applicability of reported sensor also was examined in the water sample.

Acknowledgements

The authors gratefully acknowledge the financial support of the Ministry of Science and Technology, Taiwan through contract Nos: MOST106-2113-M-027-004 and MOST106-2221-E-182-021. The financial support from the Chung Gung Memorial Hospital through contract no. BMRP 280 to B.S. Lou is also acknowledged. The authors extend their appreciation to the Deanship of Scientific Research at King Saud University for funding this work through research group no. (RG-195).

Appendix A. Supplementary material

Supplementary data associated with this article can be found, in the online version, at https://doi.org/10.1016/j.jcis.2017.12.016.

References

[1] M.H. Habibi, A.H. Habibi, M. Zendehdel, M. Habibi, Dye-sensitized solar cell characteristics of nanocomposite zinc ferrite working electrode: effect of composite precursors and titania as a blocking layer on photovoltaic performance, Spectrochim. Acta Mol. Biomol. Spectrosc. 110 (2013) 226–232.
[2] P. Guo, Z. Li, S. Liu, J. Xue, G. Wu, H. Li, X.S. Zhao, Electrochemical properties of colloidal nanocrystal assemblies of manganese ferrite as the electrode materials for supercapacitors, J. Mater. Sci. 52 (2017) 5359–5365.
[3] L. Durai, B. Moorthy, C.I. Thomas, D.K. Kim, K.K. Bharathi, Electrochemical properties of $BiFeO_3$ nanoparticles: anode material for sodium-ion battery application, Mater. Sci. Semicond. Process. 68 (2017) 165–171.
[4] A. Singh, A. Singh, S. Singh, P. Tandon, Fabrication of copper ferrite porous hierarchical nanostructures for an efficient liquefied petroleum gas sensor, Sens. Actuat. B 244 (2017) 806–814.
[5] L. Zhang, T. Hong, Y. Li, C. Xia, CaO effect on the electrochemical performance of lanthanum strontium cobalt ferrite cathode for intermediate-temperature solid oxide fuel cell, Int. J. Hydrogen Energy 42 (2017) 17242–17250.
[6] R. Nivetha, C. Santhosh, P. Kollu, S.K. Jeong, A. Bhatnagar, A.N. Grace, Cobalt and nickel ferrites based graphene nanocomposites for electrochemical hydrogen evolution, J. Magn. Magn. Mater. (2017), https://doi.org/10.1016/j.jmmm.2017.05.083.
[7] J.Q. Dai, J.W. Xu, J.H. Zhu, Thermodynamic stability of $BiFeO_3$ (0001) surfaces from ab initio theory, ACS Appl. Mater. Interfaces 9 (2017) 3168–3177.
[8] J. Zou, J. Jiang, Y. Zhang, J. Ma, Q. Wan, A comparative study of the optical, magnetic and electrocatalytic $BiFeO_3$ with different morphologies, Mater. Lett. 72 (2012) 134–136.
[9] J. Zou, M.N. Anjum, J. Yan, L. Huang, J. Chen, Y. Zhang, Synthesis and characterization of wafer-like $BiFeO_3$ with efficient catalytic activity, Solid State Sci. 13 (2011) 1779–1785.
[10] J. Zou, V. Gong, J. Ma, L. Li, J. Jiang, Efficient catalytic activity $BiFeO_3$ nanoparticles prepared by novel microwave-assisted synthesis, J. nanosci. Nanotech. 15 (2015) 1304–1311.
[11] K.L.D. Silva, D. Menzel, A. Feldhoff, C. Kubel, M. Bruns, A. Paesano, J.A. Duvel, M. Wilkening, M. Ghafari, H. Hahn, F.J. Litterst, P. Heitjans, K.D. Becker, V.S. Mechano, Synthesized $BiFeO_3$ nanoparticles with highly reactive surface and enhanced magnetization, J. Phys. Chem. C 115 (2011) 7209–7217.
[12] S. Bharathkumar, M. Sakar, S. Balakumar, Experimental evidence for the carrier transportation enhanced visible light driven photocatalytic process in bismuth ferrite ($BiFeO_3$) one-dimensional fiber nanostructures, J. Phys. Chem. C 120 (2016) 18811–18821.
[13] Y. Wang, G. Xu, L. Yang, Z. Ren, X. Wei, W. Weng, P. Du, G. Shen, G. Han, Hydrothermal synthesis of single-crystal bismuth ferrite nano flakes assisted by potassium nitrate, Ceram. Int. 35 (2009) 1285–1287.
[14] B. Sun, L. Wei, H.L.P. Chen, White-light-controlled ferromagnetic and ferroelectric properties of multiferroic single crystalline $BiFeO_3$ nanoflowers at room temperature, J. Mater. Chem. C 2 (2014) 7547–7551.
[15] J.P. Zhou, R.J. Xiao, Y.X. Zhang, Z. Shi, G.Q. Zhu, Novel behaviors of single-crystalline $BiFeO_3$ nanorods hydrothermally synthesized under magnetic field, J. Mater. Chem. C 3 (2015) 6924–6931.
[16] J.T. Han, Y.H. Huang, X.J. Wu, C.L. Wu, W. Wei, B. Peng, W. Huang, J.B.G. Enough, Tunable synthesis of bismuth ferrites with various morphologies, Adv. Mater. 18 (2006) 2145–2148.
[17] P. Li, L. Li, M. Xu, Q. Chen, Y. He, Enhanced photocatalytic property of $BiFeO_3$/N-doped graphene composites and mechanism insight, Appl. Surf. Sci. 396 (2017) 879–887.
[18] S.Y. Yang, F. Zavaliche, L.M. Ardabili, V. Vaithyanathan, D.G. Schlom, Y.J. Lee, Y. H. Chu, M.P. Cruz, Q. Zhan, T. Zhao, R. Ramesh, Metal organic chemical vapor deposition of lead-free ferroelectric $BiFeO_3$ films for memory applications, Appl. Phys. Lett. 87 (2005) 102903.
[19] Z.L. Hou, H.F. Zhou, L.B. Kong, H. BoJin, X. Qi, M.S. Cao, Enhanced ferromagnetism and microwave absorption properties of $BiFeO_3$ nanocrystals with Ho substitution, Mater. Lett. 84 (2012) 110–113.
[20] D. Sando, A. Agbelele, D. Rahmedov, J. Liu, P. Rovillain, C. Toulouse, I.C. Infante, A.P. Pyatakov, S. Fusil, E. Jacquet, C. Carrétéro, C. Deranlot, S. Lisenkov, D. Wang, J.M.L. Breton, M. Cazayous, A. Sacuto, J. Jurassic, A.K. Zvezdin, L. Bellaiche, B. Dkhil, A. Barthélémy, M. Bibes, Crafting the magnonic and spintronic response of $BiFeO_3$ films by epitaxial strain, Nat. Mater. 12 (2013) 641–646.
[21] K.A. McDonnell, N. Wadnerkar, N.J. English, M. Rahman, D. Dowling, Photo-active and optical properties of bismuth ferrite ($BiFeO_3$): an experimental and theoretical study, Chem. Phys. Lett. 572 (2013) 78–84.
[22] K.V. Jadhav, M.K. Zate, S. Liu, M. Naushad, R.S. Mane, K.N.H. Hui, S.H. Han, Mixed-phase bismuth ferrite Nano flake electrodes for super capacitor application, Appl. Nanosci. 6 (2016) 511–519.
[23] J. Xie, C. Guo, P. Yang, X. Wang, D. Liu, C.M. Li, Bi-functional ferroelectric $BiFeO_3$ passivated $BiVO_4$ photoanode for efficient and stable solar water oxidation, Nano Energy 31 (2017) 28–36.
[24] A. Sarkar, G.G. Khan, A. Chaudhuri, A. Das, K. Mandal, Multifunctional $BiFeO_3$/TiO_2 nano-heterostructure: photo-ferroelectricity, rectifying transport, and nonvolatile resistive switching property, Appl. Phys. Lett. 108 (2016) 033112.
[25] M. Sobhan, Q. Xu, A. Katoch, F. Anariba, S.S. Kim, W. Ping, O_2 sensing dynamics of $BiFeO_3$ nanofibers: effect of minor carrier compensation, Nanotechnology 26 (2015) 175501.
[26] R.Y.A. Hassan, R.O. El-Attar, H.N.A. Hassan, M.A. Ahmed, E. Khaled, Carbon nanotube-based electrochemical biosensors for determination of *Candida albicans*'s quorum sensing molecule, Sens. Actuat. B 244 (2017) 565–570.
[27] M. Sakthivel, R. Madhu, M. Sivakumar, S.M. Chen, N. Miyamoto, Y.S. Hou, V. Veeramani, A facile synthesis of Cd (OH)-rGO nano composites for the practical electrochemical detection of acetaminophen, Electroanalysis 28 (2016) 1–8.
[28] M.R. Nasrabadi, A. Khoshroo, M.M. Ardakani, Electrochemical determination of diazepam in real samples based on fullerene-functionalized carbon nanotubes/ionic liquid nanocomposite, Sens. Actuat. B 240 (2017) 125–131.
[29] J.M.M. Avila, S.S. Valdes, I.Y. Flores, O.S.R. Fernandez, M.G.N. Velazquez, E.H. Hernandez, S.F.F.A. Gallardo, T.L.B. Ramırez, A.M. Cepeda, P.G. Lafleur, Influence of carbon nanofiber functionalization and compatibilizer on the physical properties of carbon nanofiber reinforced polypropylene nanocomposites, Polym. Compos. (2017), https://doi.org/10.1002/pc.24380.
[30] Y. Yang, M.C. Gupta, K.L. Dudley, R.W. Lawrence, Conductive carbon nanofiber polymer foam structures, Adv. Matter 17 (2005) 1999–2003.
[31] R.R. Mitchell, B.M. Gallant, C.V. Thompsona, C.V. Horn, All-carbon-nanofiber electrodes for high-energy rechargeable Li–O_2 batteries, Energy Environ. Sci. 4 (2011) 2952.

[32] G. Ye, X. Zhu, S. Chen, D. Li, Y. Yin, Y. Lu, S.K.D. Yang, Nanoscale engineering of nitrogen-doped carbon nanofiber aerogels for enhanced lithium ion storage, J. Mater. Chem. A 5 (2017) 8247.
[33] L.F. Chen, Y. Lu, L. Yu, X.W.D. Lou, Designed formation of hollow particle-based nitrogen-doped carbon nanofibers for high-performance supercapacitors, Energy Environ. Sci. http://doi.org/10.1039/c7ee00488e.
[34] J. Liu, Y.T. Kuo, Y.T. Klabunde, C. Rochford, J. Wu, J. Li, Novel dye-sensitized solar cell architecture using TiO_2-coated vertically aligned carbon nanofiber arrays, ACS Appl. Mater. Interfaces 1 (2009) 1645–1649.
[35] S. Gupta, A. Yadav, N. Verma, Simultaneous Cr (VI) reduction and bioelectricity generation using microbial fuel cell based on alumina-nickel nanoparticles-dispersed carbon nanofiber electrode, Chem. Eng. J. 307 (2017) 729–738.
[36] J. Huang, Y. Liu, T. You, Carbon nanofiber based electrochemical biosensors: a review, Solid State Sci. Anal. Methods 2 (2010) 202–211.
[37] C. Zhu, G. Yang, H. Li, D. Du, Y. Lin, Electrochemical sensors and biosensors based on nanomaterials and nanostructures, Anal. Chem. 87 (2015) 230–249.
[38] H. Jiang, S. Wang, W. Deng, Y. Zhanga, Y. Tan, Q. Xie, M. Ma, Graphene-like carbon nanosheets as a new electrode material for electrochemical determination of hydroquinone and catechol, Talanta 164 (2017) 300–306.
[39] Q. Chen, X. Li, X. Min, D. Cheng, J. Zhou, Y. Li, Z. Xie, P. Liu, W. Cai, C. Zhang, Determination of catechol and hydroquinone with high sensitivity using MOF-graphene composites modified electrode, J. Electroanal. Chem. 789 (2017) 114–122.
[40] S. Palanisamy, K. Thangavelu, S.M. Chen, V. Velusamy, T.W. Chen, R.S. Kannan, Preparation and characterization of a novel hybrid hydrogel composite of chitin stabilized graphite: application for selective and simultaneous electrochemical detection of dihydroxybenzene isomers in water, J. Electroanal. Chem. 785 (2017) 40–47.
[41] M. Wei, Y. Liu, Z.Z. Gu, Z.D. Li, Electrochemical detection of catechol on boron-doped diamond electrode modified with Au/TiO_2 nanorod composite, J. Chin. Chem. Soc. 58 (2011) 516–521.
[42] Q. Ye, F. Yan, D. Kong, J. Zhang, X. Zhou, J. Xu, L. Chen, Constructing a fluorescent probe for specific detection of catechol based on 4-carboxyphenylboronic acid-functionalized carbon dots, Sens. Actuat. B 250 (2017) 712–720.
[43] N. Schweigert, A.J.B. Zehnder, R.I.L. Eggen, Chemical properties of catechols and their molecular modes of toxic action in cells, from microorganisms to mammals, Environ. Microb. 3 (2001) 81–91.
[44] H.L. White, M.N. McLeod, J.R. Davidson, Catechol O-methyltransferase in red blood cells of schizophrenic, depressed, and normal human subjects, Brit. J. Psychiat. 128 (1976) 184.
[45] H. Cui, C. He, G. Zhao, Determination of polyphenols by high-performance liquid chromatography with inhibited chemiluminescence detection, J. Chromatogr. A 855 (1999) 171–179.
[46] A.I. Yaropolov, A.N. Kharybin, J. Ermneus, G.M. Varga, L. Gorton, Flow-injection analysis of phenols at a graphite electrode modified with co-immobilised lactase and tyrosinase, Anal. Chim. Acta 308 (1995) 137–144.
[47] E.C. Figueiredo, C.R.T. Tarley, L.T. Kubota, S. Rath, M.A.Z. Arruda, On-line molecularly imprinted solid phase extraction for the selective spectrophotometric determination of catechol, Microchem. J. 85 (2007) 290–296.
[48] V. Sindelar, M.A. Cejas, F.M. Raymo, W. Chen, S.E. Parker, A.E. Kaifer, Supramolecular assembly of 2,7-dimethyldiazapyrenium and cucurbituril: a new fluorescent host for detection of catechol and dopamine, Chem. Eur. J. 11 (2005) 7054–7059.
[49] M. Sivakumar, M. Sakthivel, S.M. Chen, P. Veerakumar, S.B. Liu, Sol-gel synthesis of carbon-coated $LaCoO_3$ for effective electrocatalytic oxidation of salicylic acid, Chem ElectroChem 4 (2017) 1–7.
[50] T. Kokulnathan, N. Raja, S.M. Chen, W.C. Liao, Nanomolar electrochemical detection of caffeic acid in fortified wine samples based on gold/palladium nanoparticles decorated graphene flakes, J. Colloid Interface Sci. 501 (2017) 77–85.
[51] M. Sivakumar, M. Sakthivel, S.M. Chen, One pot synthesis of CeO_2 nanoparticles on a carbon surface for the practical determination of paracetamol content in real samples, RSC Adv. 6 (2016) 104–227.
[52] K. Thangavelu, S. Palanisamy, S.M. Chen, V. Velusamy, T.W. Chen, S.K. Ramaraj, Electrochemical determination of caffeic acid in wine samples using reduced graphene oxide/polydopamine composite, J. Electrochem. Soc. 14 (2016) 726–731.
[53] F. Pashaloo, S. Bazgir, M. Tamizifar, M. Faghihisani, S. Zakerifar, Preparation and characterization of carbon nanofibers via electro spun PAN nanofibers, Text. Sci. Technol. J. 3 (2008) 2.
[54] S. Palanisamy, K. Thangavelu, S.M. Chen, B. Thirumalraj, X.H. Liu, Preparation and characterization of gold nanoparticles decorated on graphene oxide@polydopamine composite: application for sensitive and low potential detection of catechol, Sens. Actuat. B 233 (2016) 298–306.
[55] N. Aravindan, S. Preethi, M.V. Sangaranarayanan, Non-enzymatic selective determination of catechol using copper microparticles modified polypyrrole coated glassy carbon electrodes, J. Electrochem. Soc. 164 (2017) 274–284.
[56] H. Wang, J. Qu, Y. Wang, S. Li, J. Qu, Determination of catechol based on gold/Ni $(OH)_2$ nanocomposites supported on reduced graphene oxide via a one-step wet-chemical method, Anal. Methods 9 (2017) 338–344.
[57] X. Ma, Z. Liu, C. Qiu, H. Ma, Simultaneous determination of hydroquinone and catechol based on glassy carbon electrode modified with gold-graphene nanocomposite, Microchim. Acta 180 (2013) 461.
[58] W. Liu, L. Wu, X. Zhang, Highly-selective electrochemical determination of catechol based on 3-aminophenylboronic acid-3,4,9,10-perylene tetracarboxylic acid functionalized carbon nanotubes modified electrode, J. Chen Anal. Methods 6 (2014) 718–724.
[59] Y. Wang, J. Qu, H. Li, Y. Dong, J. Qu, Simultaneous determination of hydroquinone and catechol using a glassy carbon electrode modified with gold nanoparticles, ZnS/NiS@ZnS quantum dots and L-cysteine, Microchim. Acta 182 (2015) 2277–2283.
[60] Y. Zhang, S. Xiao, J. Xie, Z. Yang, P. Pang, Y. Gao, Simultaneous electrochemical determination of catechol and hydroquinone based on graphene–TiO_2 nanocomposite modified glassy carbon electrode, Sens. Actuat. B 204 (2014) 102–108.
[61] Q. Guo, M. Zhang, G. Zhou, L. Zhu, Y. Feng, H. Wang, B. Zhong, H. Hou, Highly sensitive simultaneous electrochemical detection of hydroquinone and catechol with three-dimensional N-doping carbon nanotube film electrode, J. Electroanal. Chem. 760 (2016) 15–23.
[62] T. Gan, J. Sun, K. Huang, L. Song, Y. Li, A graphene oxide–mesoporous MnO_2 nanocomposite modified glassy carbon electrode as a novel and efficient voltammetric sensor for simultaneous determination of hydroquinone and catechol, Sens. Actuat. B 177 (2013) 412–418.
[63] M. Elancheziyan, D. Manoj, D. Saravanakumar, K. Thenmozhi, S. Senthilkumar, Amperometric sensing of catechol using a glassy carbon electrode modified with ferrocene covalently immobilized on graphene oxide, Microchim. Acta 184 (2017) 2925–2932.
[64] L. Liu, Z. Ma, X. Zhu, L.A. Alshahrani, S. Tie, J. Nan, A glassy carbon electrode modified with carbon nano-fragments and bismuth oxide for electrochemical analysis of trace catechol in the presence of high concentrations of hydroquinone, Microchim. Acta 183 (2016) 3293–3301.
[65] Y.H. Huang, J.H. Chen, X. Sun, Z.B. Su, H.T. Xing, S.R. Hu, W. Weng, H.X. Guo, W. B. Wu, Y.S. He, One-pot hydrothermal synthesis carbon nanocages-reduced graphene oxide composites for simultaneous electrochemical detection of catechol and hydroquinone, Sens. Actuat. B 212 (2015) 165–173.
[66] Z. Huo, Y. Zhou, Q. Liu, X. He, Y. Liang, M. Xu, Sensitive simultaneous determination of catechol and hydroquinone using a gold electrode modified with carbon nanofibers and gold nanoparticles, Microchim. Acta 173 (2011) 119–125.
[67] Y. Dang, Y. Zhai, L. Yang, Z. Peng, N. Cheng, Y.Z. Zhou, Selective electrochemical detection of hydroquinone and catechol at a one-step synthesized pine needle-like nano-$CePO_4$ modified carbon paste electrode, RSC Adv. 6 (2016) 83994–84002.
[68] S. Li, R. Nechache, I.A.V. Davalos, G. Goupil, L. Nikolova, M. Nicklaus, J. Laverdiere, A. Ruediger, F. Rosei, Ultrafast microwave hydrothermal synthesis of $BiFeO_3$ nanoplates, J. Am. Ceram. Soc. 10 (2013) 3155–3162.
[69] M.S. Ahmed, S. Jeon, Electrochemical activity evaluation of chemically damaged carbon nanotube with palladium nanoparticles for ethanol oxidation, J. Power Sources 282 (2015) 479–488.
[70] J. Cai, Y. Huang, B. Huang, S. Zheng, Y. Guo, Enhanced activity of Pt nanoparticle catalysts supported on manganese oxide-carbon nanotubes for ethanol oxidation, Int. J. Hydrogen Energy 39 (2014) 798–807.
[71] Y. Umasankar, A. Prakash Periasamy, S.M. Chen, Electrocatalysis and simultaneous determination of catechol and quinol by poly(malachite green) coated multiwalled carbon nanotube film, Anal. Biochem. 411 (2011) 71–79.
[72] S. Palanisamy, S.K. Ramaraj, S.M. Chen, T.W. Chiu, V. Velusamy, T.C.K. Yang, T. W. Chen, S. Selvam, One pot electrochemical synthesis of poly(melamine) entrapped gold nanoparticles composite for sensitive and low level detection of catechol, J. Colloid Interface Sci. 496 (2017) 364–370.
[73] S. Palanisamy, K. Thangavelu, S.M. Chen, B. Thirumalraj, X.H. Liu, Preparation and characterization of gold nanoparticles decorated ongraphene oxide@polydopamine composite: application for sensitiveand low potential detection of catechol, Sens. Actuat. B 233 (2016) 298–306.
[74] R. Madhu, S. Palanisamy, S.M. Chen, S. Piraman, A low temperature synthesis of activated carbon from the bio waste for simultaneous electrochemical determination of hydroquinone and catechol, J. Electroanal. Chem. 727 (2014) 84–90.
[75] S. Palanisamy, S.K. Ramaraj, S.M. Chen, T.C.K. Yang, P. Yi-Fan, T.W. Chen, V. Velusamy, S. Selvam, A novel laccase biosensor based on laccase immobilize graphene-cellulose microfiber composite modified screen-printed carbon electrode for sensitive determination of catechol, Sci. Rep. 7 (2017) 41214.
[76] S. Palanisamy, S.K. Ramaraj, S.M. Chen, V. Velusamy, T.C.K. Yang, T.W. Chen, Voltammetric determination of catechol based on a glassy carbon electrode modified with a composite consisting of graphene oxide and polymelamine, Microchim. Acta 184 (2017) 1051–1057.
[77] Xue-Lian Yu, Yu Wang, Yong-Ming Hu, Chuan-Bao Cao, H.L.W. Chan, Gas-sensing properties of perovskite $BiFeO_3$ nanoparticles, J. Am. Ceram. Soc. 92 (12) (2009) 3105–3107.
[78] S. Mallakpour, S. Soltanian, Surface functionalization of carbon nanotubes: fabrication and applications, RSC Adv. 6 (2016) 109916–109935.